CrossMark

# Synthesis, characterization and comparative studies of dual doped ZnO nanoparticles for photocatalytic applications

R. Bomila[1] · S. Suresh[2] · S. Srinivasan[1]

## Abstract

Pure and dual doped ZnO nanoparticles were synthesized via the wet chemical method. The synthesized samples were characterized by XRD, HR-SEM/EDS, HR-TEM, UV–Vis, PL, FT-IR, and FT-Raman spectral measurements. The prepared ZnO nanoparticles exhibit a hexagonal wurtzite structure and [Ce–La, La–Gd, Gd–Ce] rare earth dual doped ZnO nanoparticles was confirmed from the shift in XRD peaks position, cell parameter and also changes in the peaks intensity. HR-SEM/EDS and HR-TEM show spherical in shape with less agglomeration on the surface of all samples and the images are clearly revealed that the particle size ∼ 40 nm (PZ), 14 nm (ZCL3), 16 nm (ZLG3) and 28 nm (ZGC3). UV–Vis spectra show a strong Ultraviolet region absorbance for ZCL3 sample with the low Energy band gap value of 2.81 eV. The presences of the functional group and molecular vibrations are characterized by employing the FT-IR and FT-Raman spectra. From the PL spectra, it was found that the peak position of all samples produces a visible emission. The photocatalytic performance of the synthesized doped nanoparticles found to exhibit better degradation of MB dye under solar irradiation ZCL3 showed an increase in the photo catalytic decolorization efficiency. The bactericidal activity of dual doped ZnO nanoparticles was investigated against Gram-positive and Gram-negative bacteria and compare with standard ampicillin. We observe that ZCL3 sample have excellent antibacterial activity against Gram-negative bacteria (*P. mirabilis*) and the mean zone of inhibition ∼ 20 mm.

## 1 Introduction

In recent years, industrial pollutants found in the environment particularly air and water poses serious health hazards to the human life. Therefore, the developments of the cost-effective method to control water pollution consider top priority in current research. Semiconducting nanoparticles have attracted wide attention in this area due to their unique structural and functional properties which are utilized for potential applications in energy and environmental nanotechnology [1]. Semiconductors are widely used as a photocatalyst to convert harmful toxic organic pollutants into harmless elements. Hence, it is used to eliminate environmental pollutants and attracted the researchers to work on the area a great deal of interest in the recent past [2]. Among the vast majority of semiconductor photocatalysts,

Due to the excellent electric, optical and oxidation resistance properties of ZnO, it serves as a promising component in cosmetics and biological applications [3]. It also acts as a promising host material for both rare earth ions as well as a transition–metal ions due to its wide band gap of 3.37 eV and high free exciton binding energy of 60 meV [4]. A suitable method for preparing ZnO at low operating cost, working at ambient temperature, smaller size range and better properties are a challenge for scientists. It exhibits higher quantum efficiency and photocatalytic activity than $TiO_2$ in certain cases [5]. Hence, the photocatalytic activity of ZnO has to be enhanced than the other materials by employing various strategies. One of the important strategies in improving the photocatalytic properties is doping the metal oxides which eventually results in the variation of surface area and the incorporation of dopant ions generate lattice defects and modify bandgap energy and its visible light response [6–8]. Consequently, doping of transition metals, noble metals and non-metal is a very expedient way to improve the photocatalytic activity. Much rare earth doped ZnO photocatalyst was used such as Ce [9], Dy [10], La [11, 12] and Nd [13] for the photodegradation of organic pollutants. A literature survey on the photocatalytic properties and antibacterial activity

✉ S. Srinivasan
 dr_s_srinivasan@yahoo.com

1 Department of Physics, Presidency College, Chennai, Tamil Nadu 600005, India

2 Department of Physics, Saveetha Engineering College, Thandalam, Chennai, Tamil Nadu 602105, India

of RE [Ce, La, Gd] dual doped ZnO nanoparticles is very limited. This motivated us to systematically study the photocatalytic and antibacterial activity of RE [Ce–La, La–Gd, Gd–Ce] dual doped ZnO nanoparticles. Rare earth doped ZnO nanoparticles can be synthesized by many techniques such as pulsed laser deposition [14], hydrothermal method [15], ball milling method [16], sonochemical method [17]. To date, a number of research workers have reported the fabrication of nanostructured with the cube, flower, rod, spherical and sheet-like structures [18, 19]. To best of our knowledge, there has not been any study on the combined effect of dual doped ZnO on photocatalytic and antibacterial activity. The novelty of this work lies in synthesizing and characterizing of pure and dual (Ce–La), (La–Gd), (Gd–Ce) doped ZnO nanoparticles namely (PZ, ZCL3, ZLG3, ZGC3) by a wet-chemical method for low cost and large-scale production. The role of dual doped materials on the structural, optical, photocatalytic and antibacterial activity of ZnO nanoparticles has been studied. The performed studies of dual doped materials effectively qualify in the field of photocatalytic applications.
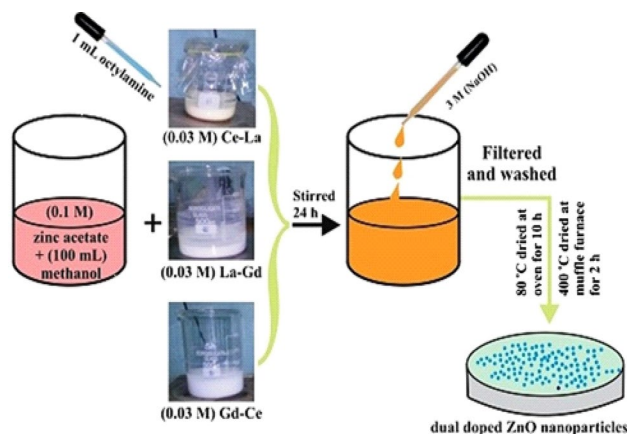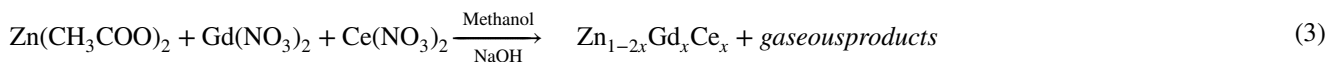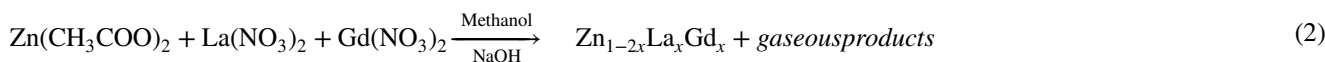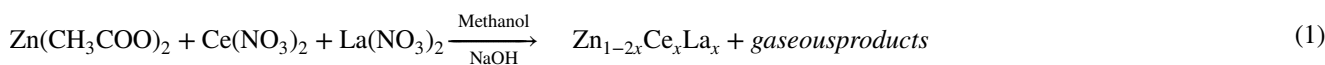


**Fig. 1** Schematic diagram of dual doped ZnO nanoparticles

2 h. For identification, the prepared samples were named as PZ (pure ZnO), ZCL3 (3 M Ce–La), ZLG3 (3 M La–Gd) and ZGC3 (3 M Gd–Ce). A schematic illustration of the experimental procedure for the synthesis is depicted in Fig. 1. The chemical reaction formulae are given in Eqs. (1–3) for dual doped ZnO nanoparticles respectively.

$$Zn(CH_3COO)_2 + Ce(NO_3)_2 + La(NO_3)_2 \xrightarrow[\text{NaOH}]{\text{Methanol}} Zn_{1-2x}Ce_xLa_x + gaseous products \tag{1}$$

$$Zn(CH_3COO)_2 + La(NO_3)_2 + Gd(NO_3)_2 \xrightarrow[\text{NaOH}]{\text{Methanol}} Zn_{1-2x}La_xGd_x + gaseous products \tag{2}$$

$$Zn(CH_3COO)_2 + Gd(NO_3)_2 + Ce(NO_3)_2 \xrightarrow[\text{NaOH}]{\text{Methanol}} Zn_{1-2x}Gd_xCe_x + gaseous products \tag{3}$$

## 2 Experimental

For the preparation of pure and dual doped ZnO nanoparticles were synthesized employing a simple wet-chemical method. In a typical synthesis of the specific amount of $Zn(ac)_2$, $Zn(ac)_2:Ce(NO_3)_3:La(NO_3)_3$, $Zn(ac)_2:La(NO_3)_3:Gd(NO_3)_3$, $Zn(ac)_2:Gd(NO_3)_3:Ce(NO_3)_3$ were dissolved in methanol and octylamine (1 mL) was added as a surfactant to control the nucleation growth. Each of them as an obtained solution was dropped into 100 ml of 3 M NaOH solution reach a pH of 12 and the stirring was continued for another 30 min. The formed glassy like white gel was allowed to age overnight. The solution was aged and then precipitates were collected out for washing by ethanol and water respectively to remove the unreacted reagents. The slurry was dried in an oven at 80 °C for 10 h. The dried powder was then annealed at 400 °C in a muffle furnace for

XRD pattern was recorded at room temperature (PAN analytical X'Pert PRO with 2θ ranging from 5° to 80°, X-ray diffractometer using CuKα irradiation (: 1.54056 Å)). High resolution scanning electron microscope (HR-SEM), High-resolution tunneling electron microscope (HR-TEM) images and energy dispersive X-ray spectroscopy analysis (EDS) were done for the samples using JEOL JSM-67001. The optical absorption and photocatalytic degradation spectra were recorded by UV–Vis absorption spectrometer (PerkinElmer T90 + Spectrophotometer). Photoluminescence measurements were carried out using JY Fluorolog-3-11 spectrometer at room temperature. FT-IR-spectra were carried out using Perkin Fourier transforms infrared spectrometer (FT-IR; JASCO, Model 6300). FT-IR Spectra were recorded in KBr dispersion in the range of 4000–400 cm$^{-1}$. FT-Raman spectra were recorded in the range of 4000–100 cm$^{-1}$ on laser Raman Microscope (Raman spectrometer Nanophoton Corporation Japan).

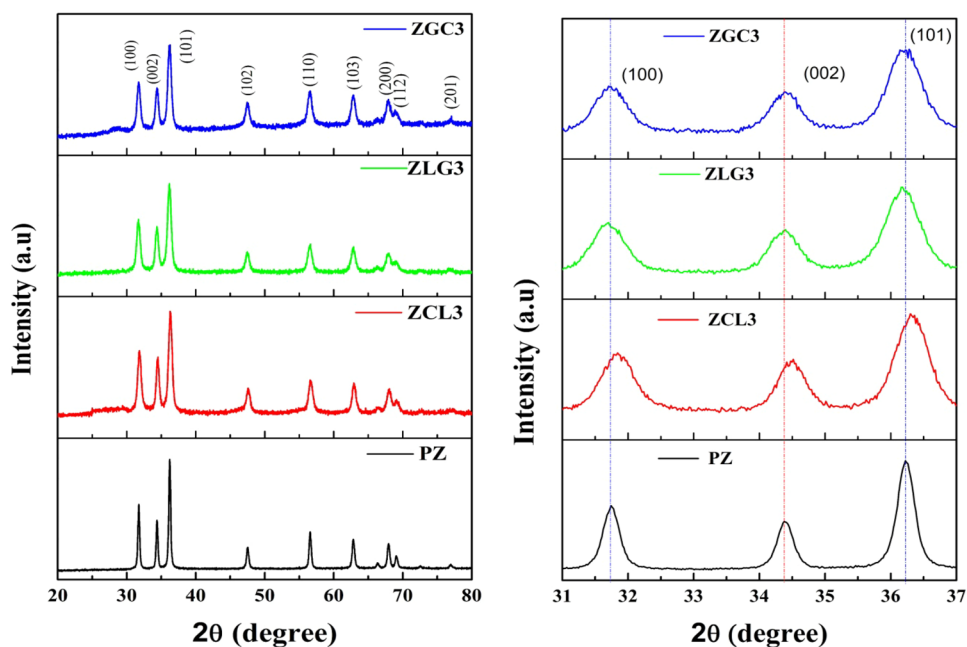**Fig. 2** XRD pattern of pure and dual doped ZnO nanoparticles



**Table 1** Structural parameters of pure and dual doped ZnO nanoparticles

| Samples | Lattice parameter values (Å) | | | Crystallite size (D) nm | Volume ($\nu$) (Å)$^3$ |
|---------|------|------|------|------|------|
| | a | c | c/a | | |
| PZ | 3.237 | 5.198 | 1.605 | 16.36 | 47.16 |
| ZCL3 | 3.244 | 5.196 | 1.601 | 9.05 | 47.37 |
| ZLG3 | 3.253 | 5.213 | 1.602 | 9.09 | 47.79 |
| ZGC3 | 3.253 | 5.210 | 1.601 | 9.61 | 47.77 |

# 3 Results and discussion

## 3.1 Structural studies

The XRD patterns of pure and dual doped ZnO nanoparticles are given in Fig. 2a. It is clearly indicated that all the samples show a hexagonal wurtzite structure. The major peaks are identified as (100), (002), (101) planes showing sharp diffraction peaks with ZnO which well matched with the standard JCPDS card (36-1451). There was a shifting of diffraction peaks towards slightly higher angle, i.e., 0.08, 0.07 and 0.04 for ZCL3, ZLG3 and ZGC3 respectively were inferred from the Fig. 2b. It might be due to the additional strain developed due to dual doped rare earth elements into the ZnO matrix [20]. The pure ZnO sample was compared with doped ZnO samples, it was noticed that the peak intensities were reduced and they are full with half maxima values were increased in the XRD patterns. It is due to the fact that dual doped rare earth ions into the ZnO lattice and hence

its crystallinity was decreased. The formation of dual doped elements can be explained by the hindered incorporation of the large ionic radii $Ce^{3+}$ (0.103 nm), $La^{3+}$ (0.115 nm) and $Gd^{3+}$ (0.093 nm) in comparison to that of $Zn^{2+}$ (0.074 nm) which makes the replacement more difficult, thus distorting the ZnO lattice [21–23]. Table 1, summarizes the structural parameters like lattice parameters, crystallite size, and volume of the pure and dual doped ZnO nanoparticles. The Scherer's formula was used to calculate the average crystallite size from the prominent obtained XRD peaks in the XRD spectra [24].

$$D = \frac{K\lambda}{\beta} \cos\theta \tag{4}$$

where $K$ is a shape constant, $\lambda$ is the wavelength of X-ray (0.1540 nm), $\beta$ is the full width at half maximum and $\theta$ is the angle of diffraction. The lattice parameters of hexagonal ZnO were calculated from the relation. The volume ($\nu$) of the unit cell of a wurtzite hexagonal lattice system has been calculated using equation [25].

$$\frac{1}{d^2} = \frac{4}{3}\left(h^2 + hk + \frac{k^2}{a^2} + \frac{l^2}{c^2}\right) \tag{5}$$

$$\nu = 0.869 \times a^2 \times c \tag{6}$$

where 'a' and 'c' are the lattice parameters, h, k and l are the Miller indices and d is the inter-planer spacing for the plane (*hkl*).

**Fig. 3** HR-SEM images of pure and dual doped ZnO nanoparticles
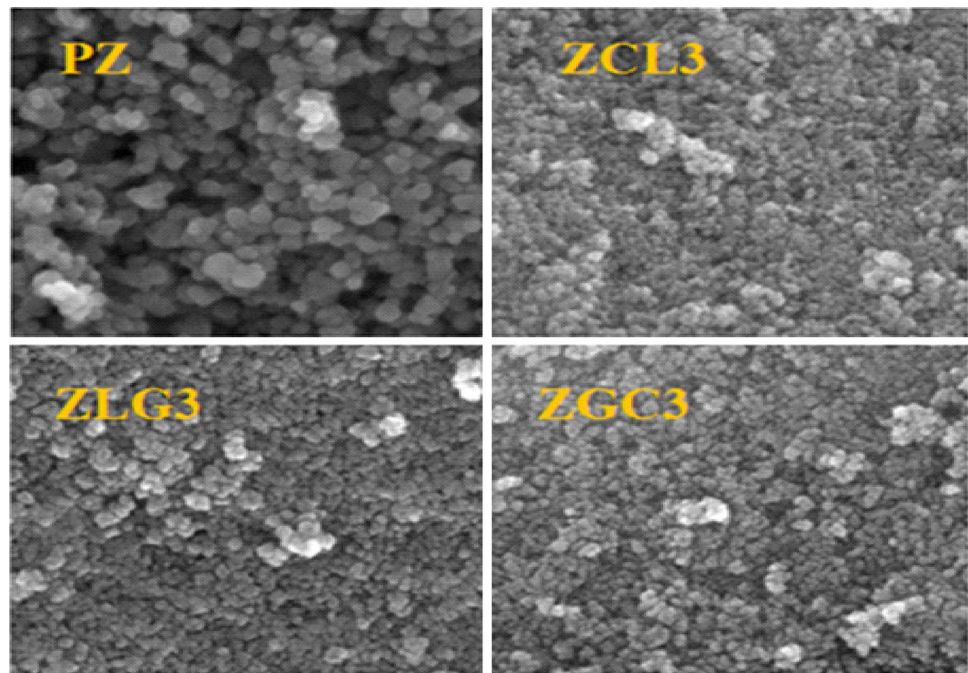


## 3.2 Morphological studies

HR-SEM images of PZ and dual doped ZnO nanoparticles are shown in Fig. 3. The PZ sample consists of randomly dispersed bigger spherical particles within the nanoscale regime. It can be seen from Fig. 3 that the sample was showed the uniform distribution of smaller spherical particles with good crystalline quality. The particle size of ZnO in pure and doped ZnO samples was also estimated from HR-SEM analysis were in good agreement with XRD results. To confirm the presence of dual doped rare earth elements and the purity of the sample was done with EDS analysis in Fig. 4. It reveals that the sample ZCL3 contains mainly four elements (Zn, O, Ce, La), ZLG3 spectrum indicates that the elements (Zn, O, La, Gd) and ZGC3 spectrum exhibits that the elements (Zn, O, Gd, Ce). It indicated that the prepared samples contain no impurity and also confirms the presence of both dual doped rare earth ions in ZnO nanoparticles.

Firsthand information about the particle size and morphology of the prepared nanocrystalline samples can be obtained by analyzing HR-TEM images of the pure and dual doped ZnO nanoparticles. The HR-TEM images clearly showed that pure and dual doped ZnO particles were in spherical in shape with almost in the uniform distribution. Figure 5 also shows the particle size of the ZnO nanoparticles incomparable with XRD and HR-SEM analysis. The nanoparticles were clearly well identified and no effective aggregations of bulk particles were formed.

## 3.3 Optical absorption studies

The UV–Vis absorption spectra of pure and dual doped ZnO nanoparticles are shown in Fig. 6. It can be seen that the optical absorption edge of pure ZnO appeared at 371 nm is due to its wide band gap energy, which suggests that the ZnO could only be activated under UV-light irradiation [26, 27]. While dual doped ZnO - like ZCL3, ZLG3 and ZGC3 showed the optical response in the range of 373, 368 and 370 nm. When the sample ZCL3 absorption decreased red shifted (2.81 eV) the observed red shifted indicates the narrow bandgap originating from the charge transfer between ZnO valence band and the rare earth ion 4f level [28]. On the other hand, ZLG3 and ZGC3 absorption peak increased blue shifted (2.92 eV) and (2.87 eV) of band gap as compared with pure ZnO nanoparticles due to quantum confinement effects [29]. The optical band gap ($E_g$) is calculated from tauc's relation.

$$(\alpha h\nu)^2 = A(h\nu - E_g)^n \tag{7}$$

where A is the function of the index of refraction and electron/hole effective mass 'α' is the optical absorbance and 'n' is a number equal to the direct gap and indirect gap semiconductors. For determination of band gap, a graph was drawn between $(\alpha h\nu)^2$ versus $h\nu$ as shown in Fig. 7. The extrapolation of a straight line on the energy ($h\nu$) axis gives a band gap for pure and dual doped ZnO nanoparticles respectively and given in Table 2.
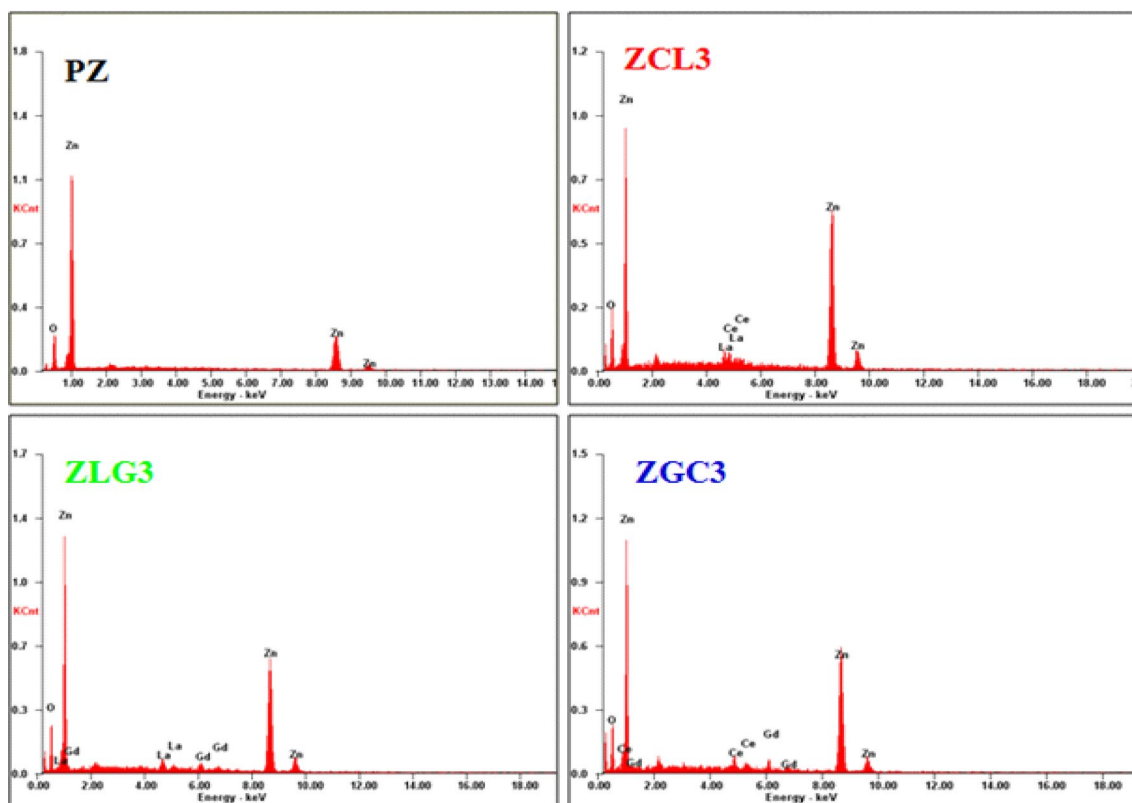
**Fig. 4** EDS pattern of pure and dual doped ZnO nanoparticles

## 3.4 Photoluminescence studies

PL spectroscopy is used to study the efficiency of recombination charge carrier trapping, migration, crystal defects and the rate of electron–hole pairs in semiconductor particles. The PL spectra of pure and dual doped ZnO nanoparticles are shown in Fig. 8. The characteristic emission band at 393 nm followed by near band edge emission was observed in all the samples. The presence of Zn interstitials in the sample was observed as a peak in the visible region at 413 nm due to electron transition. The peak centered at 436 nm confirms the presence of singly ionized oxygen vacancies which are the main sources of generation of hydroxyl radicals generation required for the photo decolorization process [28]. The emission peaks were observed at 504 nm, 528 nm and 541 nm were attributed to the radiative transition of an electron from the deep donor level of Zn interstitial to an acceptor level caused by singly ionized charged state of the defect in ZnO [29]. It is obvious all doped ZnO nanoparticles shown fewer intensity peaks as compared to pure ZnO, because of the increase in non-radiative traps produced by structural disorder [30].

## 3.5 FT-IR studies

FT-IR is one of the essential techniques to analyze the chemical bonding and functional groups present in the material and to identify the compositional elements of the material. FT-IR spectra of pure and dual doped ZnO nanoparticles are shown in Fig. 9. A very broad and strong absorption peak observed at 3425 cm$^{-1}$ was assigned to O–H stretching vibration in the hydroxyl group was seen in all the samples [31]. Due to the presence of carboxyl group, the symmetric and asymmetric C=O stretching mode of vibration was expected and assigned at 1451 cm$^{-1}$ and 1357 cm$^{-1}$ respectively in the FTIR spectra [32, 33]. The defect arises due to dual doped rare earth ions in ZnO was identified with the peak occur at 881 cm$^{-1}$ [34]. The peak 460 cm$^{-1}$ in the curves of all samples was attributed to the stretching vibration modes of Zn–O [35].

## 3.6 FT-Raman studies

Raman scattering is a technique for studying the molecular vibrational modes of semiconductor materials. Raman spectra of pure and dual doped ZnO nanoparticles in the spectral range of 200–800 cm$^{-1}$ were recorded and shown

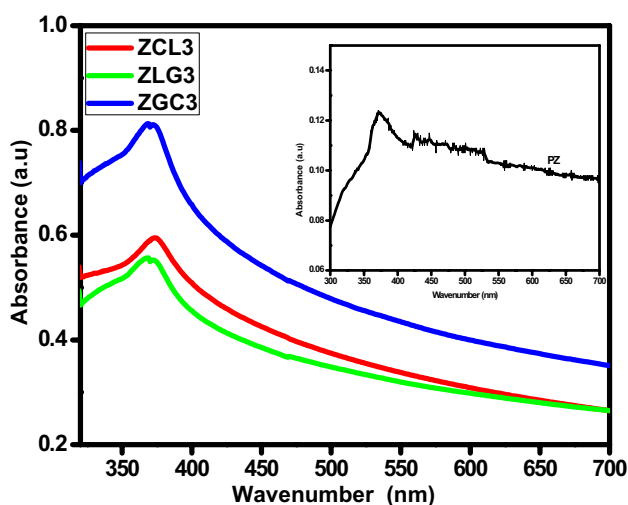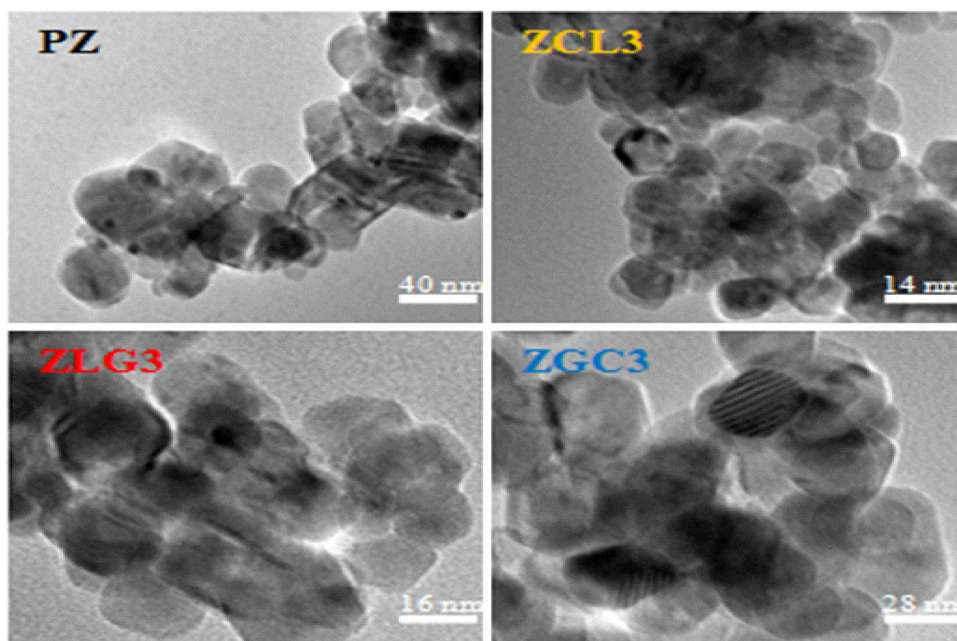**Fig. 5** HR-TEM images of pure and dual doped ZnO nanoparticles





**Fig. 6** UV–Vis absorbance spectra of dual doped ZnO nanoparticles
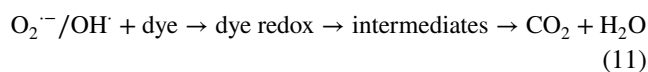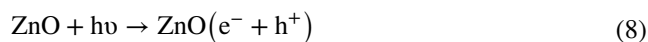
in Fig. 10. According to factor group theory, the structure of ZnO belongs to the $C_6V$ symmetry group, which predicts $2A_1$, $2E_1$, $2E_2$ and $2B_1$ modes. The peaks that at 350, 386, 438, 579, 604, 627, 706 and 756 cm$^{-1}$, for pure ZnO nanoparticles corresponding to the $E_2$ (High)-$E_2$ (Low), $A_1$ (TO), $E_2$ (High), TO + TA (M), $E_1$ (LO) and $E_2$ (Low)-$B_1$(High) fundamental phonon modes of hexagonal ZnO, respectively [36]. The intensity of both $E_2$ (low) and $E_2$ (High) modes decreases with the addition of RE compound, which can be attributed to the distortion in the crystal.

The fundamental phonon modes of ZnO in doped samples observed in the FT-Raman spectra showed a 4 cm$^{-1}$ redshift approximately in all the samples due to the cohesive bond of the lower coordinated atoms. Another cause for the redshift may be, the decrease in size relaxes the momentum thereby the Raman active modes will not be limited at the centre of the Brillouin zone. Hence, the FT-Raman studies that there was a decrease in Raman wavenumber when related to rare earth compounds than bulk material. The formation of hexagonal size in the as-synthesis ZnO nanoparticles was further supported by Raman spectroscopy.

## 3.7 Photocatalytic studies

The photocatalytic activity of pure and dual doped ZnO nanoparticles was evaluated using Methylene Blue (MB) degradation under solar light irradiation. ZnO nanoparticles exhibit photocatalytic degradation by absorbing the generation of electron–hole ($e^-/h^+$) pair. This can be achieved when the photocatalyst was irradiated with a photon of energy which equals to or higher than its band gap of the ZnO nanoparticles. Figure 11 shows the interaction of dye molecules with $e^-/h^+$ pairs and its reposition to the surface of the photocatalyst leading to redox reactions and as a sign, the dye molecules degrade as follows [37, 38].

$$ZnO + h\upsilon \rightarrow ZnO\left(e^- + h^+\right) \tag{8}$$

$$e^- + O_2 \rightarrow O_2^{\cdot -} \tag{9}$$

$$h^+ + H_2O \rightarrow OH^{\cdot} + H^+ \tag{10}$$

$$O_2^{\cdot -}/OH^{\cdot} + dye \rightarrow dye\ redox \rightarrow intermediates \rightarrow CO_2 + H_2O \tag{11}$$
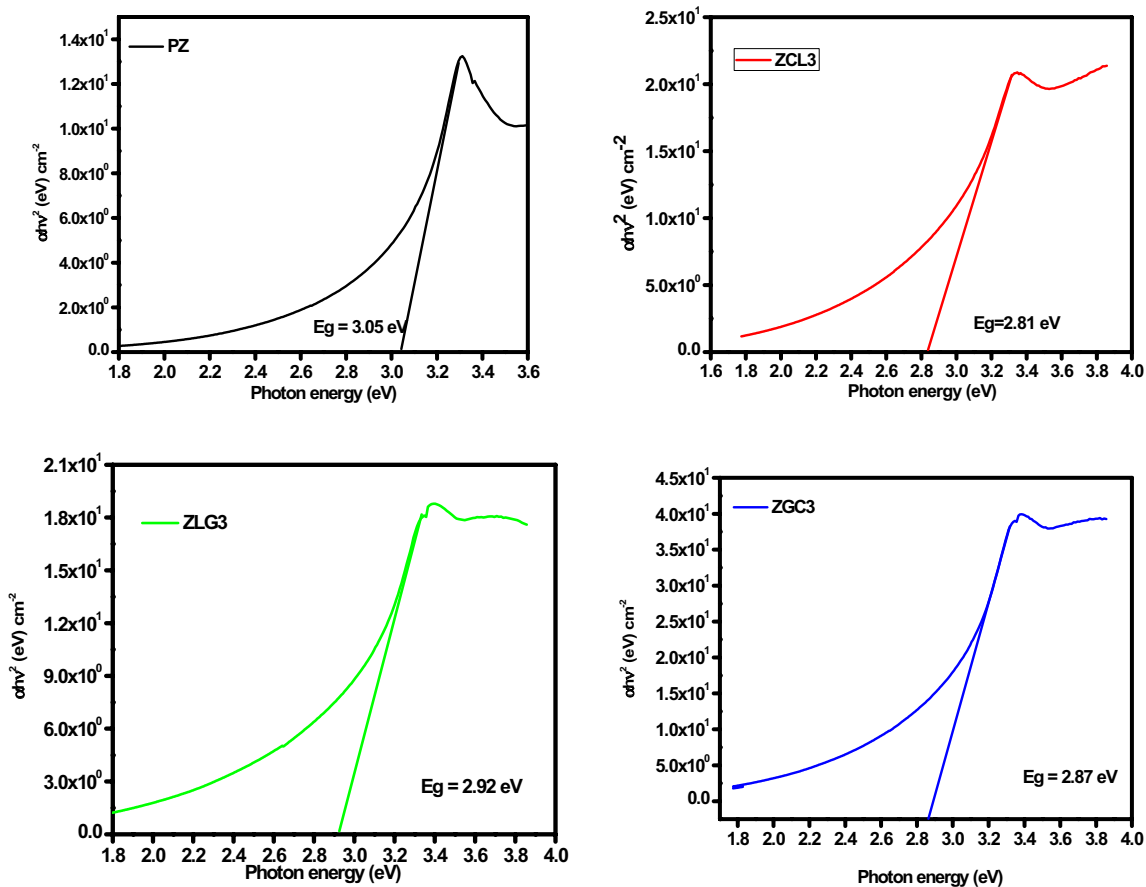
**Fig. 7** Tauc plots drawn $(\alpha h\nu)^2$ versus photon energy $(h\nu)$ of pure and dual doped ZnO nanoparticles

**Table 2** Energy band gap values for pure and dual doped ZnO nanoparticles

| S. no | Doping concentration (mole) | Absorbance value (nm) | $E_g$ (eV) |
|-------|-----------------------------|------------------------|------------|
| 1 | PZ | 366.65 | 3.05 |
| 2 | ZCL3 | 371.12 | 2.81 |
| 3 | ZLG3 | 371.99 | 2.92 |
| 4 | ZGC3 | 379.72 | 2.87 |

Highly reactive hydroxyl radicals (OH·) are formed when holes can react with water adhering to the surfaces of ZnO nanoparticles. Meanwhile, the photogenerated electrons react with oxygen to produce superoxide ($O_2^{·-}$) which in turn reacts with water to form hydrogen peroxide eventually leads to the formation of reactive hydroxyl radicals (OH·). These reactive hydroxyl radicals combined decompose organic compounds into $CO_2$, $H_2O$, and other minerals. During the photocatalytic reaction process, oxygen vacancies and defects act as active centers in capturing photo-induced electrons. As a result, photo-induced recombination
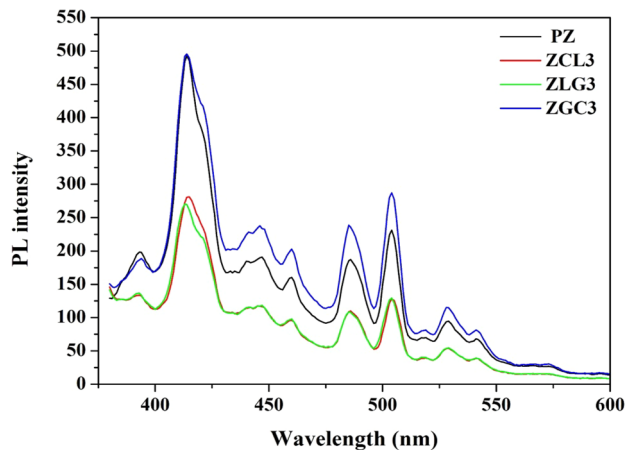


**Fig. 8** PL spectra of pure and dual doped ZnO nanoparticles

of electron and hole can be effectively inhibited. The formation of superoxide radicals ($O_2^{·-}$) occurs by absorption of $O_2$ which was induced by more oxygen vacancies the help of with photoinduced electrons [39]. These superoxide radicals are active to produce other radicals such as OH·, $H_2O_2$
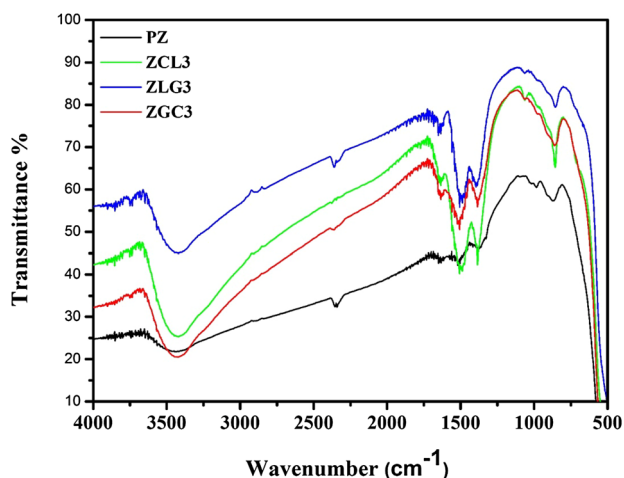
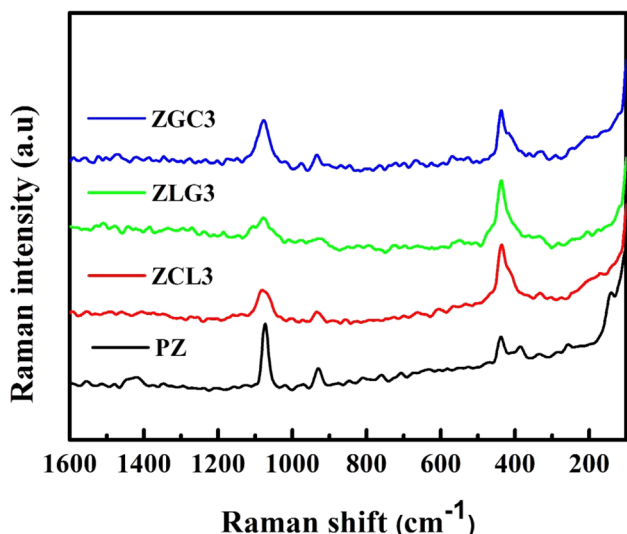**Fig. 9** FT-IR spectra of pure and dual doped ZnO nanoparticles



**Fig. 10** FT-Raman spectra of pure and dual doped ZnO nanoparticles
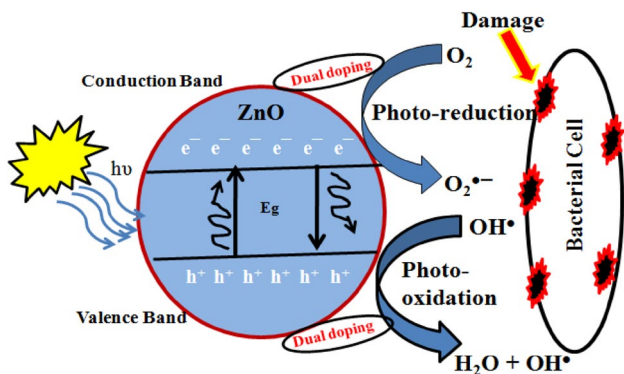


**Fig. 11** The basic mechanism of the photocatalytic activity of samples

to degrade the organic pollutants [40, 41]. Thus, this study reveals that oxygen vacancy and defects induced by dual doping in ZnO favor the photocatalytic reaction. Moreover, it was found that the photocatalytic activity can be enhanced by increased oxygen vacancy. The rate at which a pollutant was removed from the aqueous solution can be calculated with the help of rate kinetics. The reaction kinetics of MB dye was calculated using the equation [42].

$$\ln \frac{C_0}{C_t} = kt \qquad (12)$$

where $C_0$ and $C_t$ are the concentrations of the MB at $t = 0$ and at the time of t, respectively. Figure 12a shows the absorbance spectra of MB, recorded to different irradiation times in the presence of the PZ, ZCL3, ZLG3 and ZGC3 samples. Figure 12b shows the plot of concentration ratio ln ($C_0/C_t$) vs the irradiation time. The linear behavior of the plot confirms the first order kinetics of the MB degradation reaction. The kinetic parameters such as degradation rate constant (k) and linear coefficient ($R^2$) calculated from the kinetic plot for MB dye values are given in Table 3. If a photocatalyst was involved in the photo-decolorization process, it alters the absorbance by decreasing it gradually with the increase in time of irradiation. Figure 12c clearly shows that there was the decolorization efficiency of the dual doped samples is higher when compared with that of pure ZnO. Ce–La doped ZnO nanoparticles yield smaller size of ZnO. Hence, the surface to volume ratio is large when the particle size is reduced. So that it exhibits better photocatalytic activity. Moreover, ZCL3 samples showed an increase in the photocatalytic decolorization efficiency.

## 3.8 Antibacterial studies

The antibacterial activities of the pure and dual doped samples were tested against strains of Gram-positive (*Bacillus subtilis, Staphylococcus aureus*) and Gram-negative bacteria strains (*Proteus mirabilis, Salmonella typhi*) and the obtained results were shown in Fig. 13. Table 3 shows the zone of inhibition values for all the samples with standard ampicillin and the inhibition rates of all samples against antibacterial species is shown in Fig. 14. It can be seen that ZCL3 sample have good antibacterial activity against Gram-negative bacteria (*P. mirabilis*) and the mean zone of inhibition ~ 20 mm was significant when compared ampicillin. The bactericidal activity was activity was important to the material by these excited excess electrons in the conduction band and the holes created in the valence band which was the one to generate reactive oxygen vacancies (ROV). The ROVs has the capacity to penetrate into the cell membrane of microorganisms and leads to the damages the cell
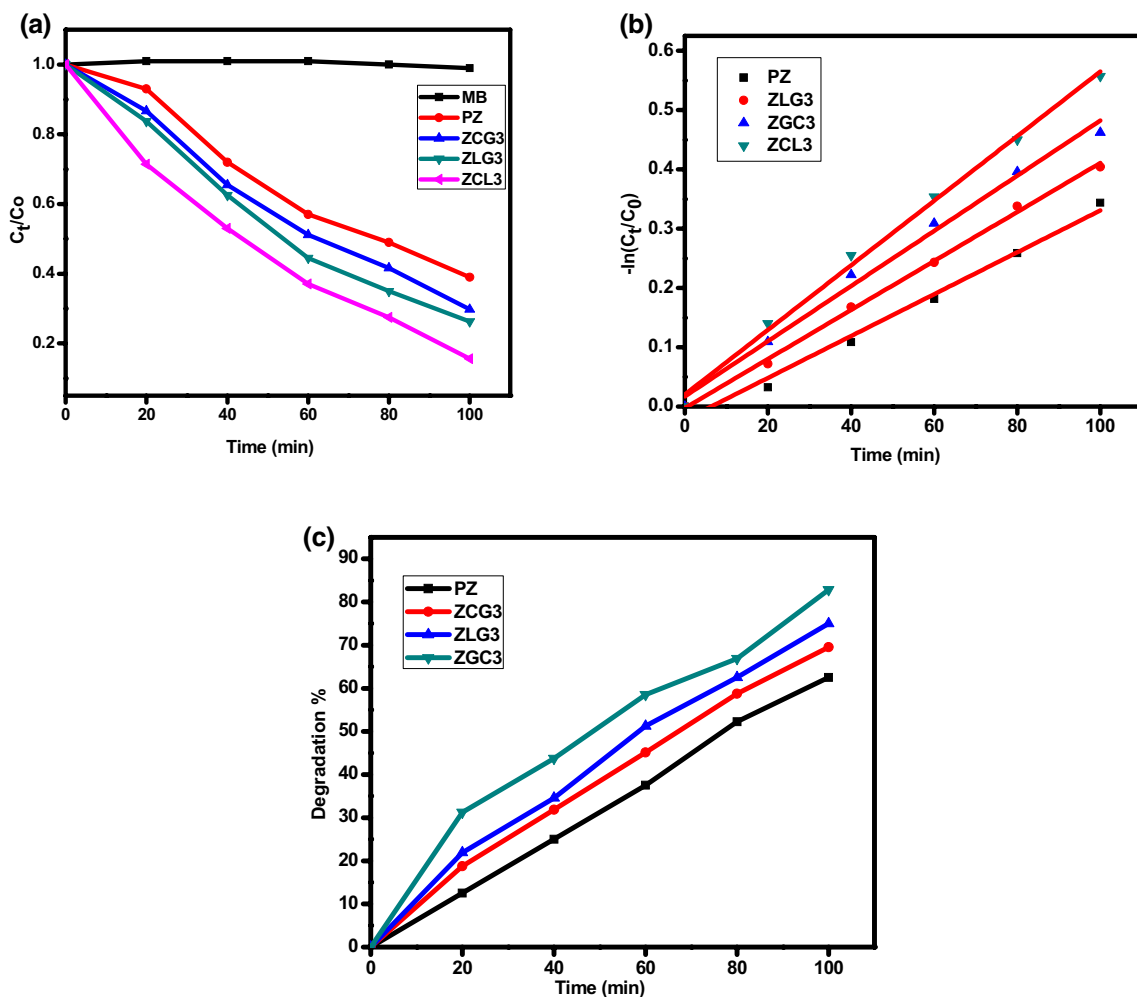
**Fig. 12** Photocatalytic activity of pure and dual doped ZnO nanoparticles, **a** photocatalytic degradation analysis, **b** photocatalytic degradation kinetic curve study and **c** photocatalytic degradation efficiency analysis
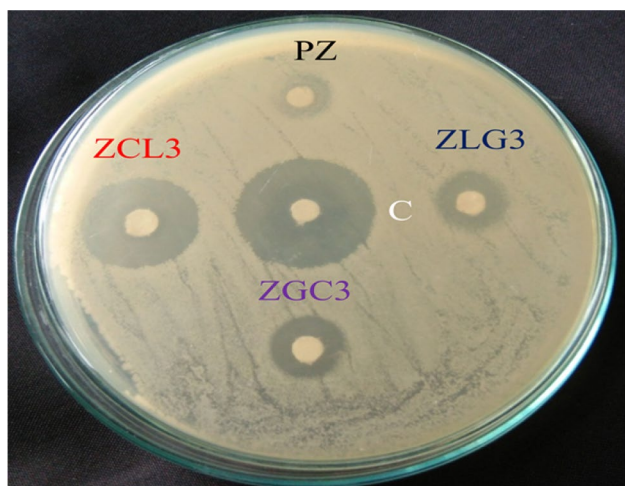


**Fig. 13** Antibacterial activity of pure and dual doped ZnO nanoparticles against *P. mirabilis*

**Table 3** Antibacterial activity of pure and dual doped ZnO nanoparticles against human pathogens

Antibacterial activities of samples were determined as zone of inhibition (in mm)

| Samples | *B. subtilis* | *S. aureus* | *P. mirabilis* | *S. typhi* |
|---|---|---|---|---|
| Ampicillin (C) | 11 | 14 | 24 | 17 |
| PZ | 5 | NA | 6 | 4 |
| ZCL3 | 8 | NA | 20 | 8 |
| ZLG3 | 6 | NA | 8 | 13 |
| ZGC3 | NA | NA | 12 | 15 |

membrane, DNA and cellular proteins [43] eventually death of the bacteria. Therefore, the samples ZCL3 have higher antibacterial efficiency than other samples. The study gave a better understanding of the bactericidal activity of ZnO
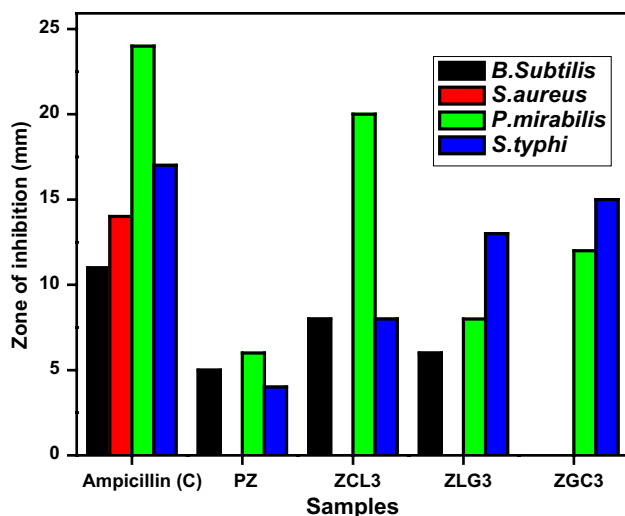
**Fig. 14** The inhibition rates of all samples against antibacterial species

nanoparticles which could be due to various properties of ZnO such as photocatalytic activity, cellular internalization, the electrostatic interaction of the nanoparticles and production of reactive oxygen species (ROS) which are responsible for antibacterial activity [44–46]. Among them, ROS generation has been considered as the dominant mechanism of antibacterial activity. ZnO with defects, created by dual doping can be activated by sunlight and generates electron–hole pairs. The holes split $H_2O$ molecules from ZnO into $OH^-$ and $H^+$ Eq. (8). Then, they produce $H_2O_2$ by reacting with a hydrogen ion. The $H_2O_2$ directly penetrate into the cell membrane and kill the bacteria whereas the other hydroxyl radicals and superoxide cannot penetrate into the cell membrane and remain in contact the outer surface of bacteria causing severe damage to proteins and lipids. In this study, the XRD, UV–Vis and photocatalytic degradation results reveal that the sample ZCL3 has the minimum particle size, more lattice defects, visible region, and higher photocatalytic degradation efficiency compared with PZ and other dual doping levels. These characteristics are beneficial for the enhancement of antibacterial activity of ZCL3 doped ZnO.

## 4 Conclusion

In this study, synthesis of dual doping RE metals such as ZCL3, ZLG3 and ZGC3 doped ZnO nanoparticles by the simple wet chemical method using octylamine as a surfactant was performed. Structural, morphological, optical properties were studied. The results conclude that ZCL3 doped ZnO nanoparticles exhibit the best photocatalytic behavior amongst the studied combinations. It may be due

to fact that particles size was lesser than other dual dopant systems as confirmed by PXRD and HR-SEM results. From the antibacterial test, it was evident ZCL3 that dual doped ZnO nanoparticles execute a better and effective antibacterial activity compared to the rest of the samples. Generation of radical oxygen vacancies (ROS) plays a vital role in imparting the toxicity mechanism on bacteria along with the electrostatic interaction between the ions and membrane. There has been a significant increase in the number of ROS which was achieved by ZCL3 doping in ZnO in showing a bactericidal activity in Gram-positive bacteria.

## References

1. B. Nowack, in *Pollution Prevention and Treatment Using Nanotechnology* (Wiley, Weinheim, 2010) https://doi.org/10.1002/9783527628155.nanotech010
2. A.K. Mishraa, D. Das, Investigation on Fe-doped ZnO nanostructures prepared by a chemical route. Mater. Sci. Eng. B **171**, 5–10 (2010)
3. M.G. Nair, M. Nirmala, K. Rekha, A. Anukaliani, Structural, optical, photocatalytic, and antibacterial activity of ZnO and Co doped ZnO nanoparticles. Mater. Lett. **65**, 1797–1800 (2011)
4. H. Gerischer, A. Heller, Photocatalytic oxidation of organic molecules at $TiO_2$ particles by sunlight in aerated water. J. Electrochem. Soc. **139**, 113–118 (1992)
5. O. Seven, B. Dindar, S. Aydemir, D. Metin, M.A. Ozinel, S. Icli, Solar photocatalytic disinfection of a group of bacteria and fungi aqueous suspensions with $TiO_2$, ZnO and Sahara desert dust. J. Photochem. Photobiol. A Chem. **165**, 103–107 (2004)
6. D.P. Singh, Synthesis and growth of ZnO nanowires. Sci. Adv. Mater. **2**, 245–272 (2010)
7. G.S. Yi, H.C. Lu, S.Y. Zhao, G. Yue, W.J. Yang, D.P. Chen, L.H. Guo, Synthesis, characterization, and biological application of size-controlled nanocrystalline $NaYF_4$:Yb, Er infrared-to-visible up-conversion phosphors. Nano Lett. **42**, 2191–2196 (2004)
8. L. Wang, R.X. Yan, Z.Y. Hao, L. Wang, J.H. Zeng, J. Bao, X. Wang, Q. Peng, Y.D. Li, Fluorescence resonant energy transfer biosensor based on upconversion-luminescent nanoparticles. Angew. Chem. Int. Ed. **44**, 6054–6057 (2005)
9. N. Kannadasan, N. Shanmugam, S. Cholan, K. Sathishkumar, G. Viruthagiri, R. Poonguzhali, The effect of $Ce^{4+}$ incorporation on structural, morphological and photocatalytic characters of ZnO nanoparticles. J. Mater. Charact. **97**, 37–42 (2014)
10. F. Gu, S.F. Wang, M.K. Lu, G.J. Zhou, D. Xu, D.R. Yuan, Structure evaluation and highly enhanced luminescence of $Dy^{3+}$ Doped ZnO nanocrystals by $Li^+$ doping via combustion method. Langmuir **20**, 3528–3531 (2004)
11. G.S. Yi, B.Q. Sun, F.Z. Yang, D.P. Chen, Y.X. Zhou, J. Cheng, Synthesis and characterization of high-efficiency nanocrystal upconversion phosphors: ytterbium and erbium codoped lanthanum molybdate. Chem. Mater. **14**, 2910–2914 (2002)
12. M.U. Staudt, S.R. Hastings-Simon, M. Nilsson, M. Afzelius, V. Scarani, R. Ricken, H. Sachet, W. Sohler, W. Tittel, N. Gisin, Fidelity of an optical memory based on stimulated photon echoes. Phys. Rev. Lett. **98**, 113601–113604 (2007)
13. G. Poongodi, R. Mohan Kumar, R. Jayavel, Structural, optical and visible light photocatalytic properties of nanocrystalline Nd doped ZnO thin films prepared by spin coating method. Ceram. Int. **41**, 4169–4175 (2015)

14. Y.R. Ryu, W.J. Kim, H.W. White, Fabrication of homostructural ZnO p–n junctions. J. Cryst. Growth **219**, 419–422 (2000)

15. P. Aneesh, K.A. Vanaja, M.K. Jayaraj, Synthesis of ZnO nanoparticles by hydrothermal method. Nanophotonic Mater. IV **6639**, 66390J (2007)

16. N. Salah, S.S. Habib, Z.H. Khan, A. Memic, A. Azam, E. Alarfaj, N. Zahed, S. Hamedi, A, High-energy ball milling technique for ZnO nanoparticles as antibacterial material. Int. J. Nanomed. **6**, 863–869 (2011)

17. E. Kowsari, Sonochemically assisted synthesis and application of hollow spheres, hollow prism, and coralline-like ZnO nanophotocatalyst. J. Nanopart. Res. **13**, 3363–3376 (2011)

18. Z.Q. Li, Y.J. Xiong, Y. Xie, Selected-control synthesis of ZnO nanowires and nanorods via a PEG-assisted route. Inorg. Chem. **42**, 8105–8109 (2003)

19. X. Wang, Y. Ding, Z. Li, J. Song, Z.L. Wang, **S**ingle-crystal mesoporous ZnO thin films composed of nanowalls. J. Phys. Chem. C **113**, 1791–1794 (2009)

20. T. Thangeeswari, M. Priya, J. Velmurugan, N. Padmanathan, Optical and magnetic properties of Yb ion-doped cobalt-based ZnO. Bull. Mater. Sci. **38**, 1389–1398 (2015)

21. C. Bingqiang, C. Weiping, From ZnO nanorods to nanoplates: chemical bath deposition growth and surface-related emissions. J. Phys. Chem. C **112**(3), 680–685 (2008)

22. C. Dewei, L. Sean, Growth and electrical properties of doped ZnO by electrochemical deposition. New J. Glass Ceram. **2**, 13–16 (2012)

23. R. Zamiri, A.F. Lemos, A. Reblo, H.A. Ahangar, J.M.F. Ferreira, Effects of rare-earth (Er, La and Yb) doping on morphology and structure properties of ZnO nanostructures prepared by wet chemical method. Ceram. Int. **40**, 523–529 (2014)

24. G. Neri, A. Bonavita, G. Rizzo, S. Galvagno, S. Capone, P. Siciliano, Electrical characterization of $Fe_2O_3$ humidity sensors doped with $Li^+$, $Zn^{2+}$ and $Au^{3+}$ ions. Sens. Actuators B **112**, 78–83 (2005)

25. K. Ueda, H. Tabata, T. Kawai, Magnetic and electric properties of transition-metal-doped ZnO films. Appl. Phys. Lett. **79**, 988 (2001)

26. S. Anandan, M. Miyauchi, Ce-doped ZnO ($Ce_x Zn_{1-x}O$) becomes an efficient visible-light-sensitive photocatalyst by co-catalyst ($Cu^{2+}$) grafting. Phys. Chem. Chem. Phys. **13**, 14937–14945 (2011)

27. J. Iqbal. X. Liu, H. Zhu, Z.B. Wu, Y. Zhang, D. Yu, R. Yu, Raman and highly ultraviolet red-shifted near band-edge properties of LaCe-co-doped ZnO nanoparticles. Acta Mater. **57**, 4790–4796 (2009)

28. K. Ravichandran, R. Mohan, B. Sakthivel, S. Varadharaja perumal, P. Devendran, T. Alagesan, K. Pandian, Enhancing the photocatalytic efficiency of sprayed ZnO thin films through double doping (Sn + F) and annealing under different ambiences. Appl. Surf. Sci. **321**, 310–317 (2014)

29. N.Y. Garces, L. Wang, L. Bai, N.C. Giles, L.E. Halliburton, G. Cantwell, Role of copper in the green luminescence from ZnO crystals. Appl. Phys. Lett. **81**, 622–624 (2002)

30. K. Ravichandran, S. Snega, N. Jabena Begum, K. Swaminathan, B. Sakthivel, L. Rene Christena, G. Chandramohan, S. Ochiai, Enhancement in the antibacterial efficiency of ZnO nanopowders by tuning the shape of the nanograins through fluorine doping. Superlattices Microstruct. **69**, 17–28 (2014)

31. J.M. Martínez, R.G. Meneses, C. Silva, Synthesis of gadolinium doped ceria ceramic powder by polymeric precursor method (Pechini). Mater. Sci. Forum **798–799**, 182–188 (2014)

32. K. Nakamoto, in *Infrared and Raman Spectra of Inorganic and Coordination Compounds: Part A: Theory and Applications in Inorganic Chemistry* (Wiley, New York, 1997)

33. S. Senthilkumar, K. Rajendran, S. Banerjee, T.K. Chini, V. Sengodan, Influence of Mn doping on the microstructure and optical property of ZnO. Mater. Sci. Semicond. Process. **11**, 6–12 (2008)

34. Y. Yang, L. Ren, C. Zhang, S. Huang, T. Liu, Facile fabrication of functionalized graphene sheets (FGS)/ZnO nanocomposites with photocatalytic property. ACS Appl. Mater. Interfaces **3**, 2779–2785 (2011)

35. H. Du, J. Ye, J. Zhang et al., A voltammetric sensor based on graphenemodified electrode for simultaneous determination of catechol and hydroquinone. J. Electroanal. Chem. **650**, 209–213 (2011)

36. J.C. Sin, J. Mun Lam, K. Teong Lee, A. Mohamed, R, Preparation of rare earth-doped ZnO hierarchical micro/nanospheres and their enhanced photocatalytic activity under visible light irradiation. Ceram. Int. **40**, 5431–5440 (2014)

37. S.M. Lam, J.C. Sin, A.Z. Abdullah, A.R. Mohamed, Green hydrothermal synthesis of ZnO nanotubes for photocatalytic degradation of methylparaben. Mater. Lett. **93**, 423–426 (2013)

38. J. Wang, Z. Wang, B. Huang, Y. Ma, Y. Liu, X. Qin, X. Zhang, Y. Dai, Oxygen vacancy induced band-gap narrowing and enhanced visible light photocatalytic activity of ZnO. ACS Appl. Mater. Interfaces **4**, 4024–4030 (2012)

39. B.N. Joshi, H. Yoon, S.H. Na, J.Y. Choi, S.S. Yoon, Enhanced photocatalytic performance of graphene-ZnO nanoplatelet composite thin films prepared by electrostatic spray deposition. Ceram. Int. **40**, 3647–3654 (2014)

40. P. Jongnavakit, P. Amornpitoksuk, S. Suwanboon, N. Ndiege, Prepara- tion and photocatalytic activity of Cu-doped ZnO thin films prepared by the sol–gel method. Appl.Surf.Sci **258**, 8192–8198 (2012)

41. Y. Liu, J. Han, W. Qiu, W. Gao, Hydrogen peroxide generation and photocatalytic degradation festrone by microstructural controlled ZnO nanorod arrays. Appl. Surf. Sci. **263**, 389–396 (2012)

42. B.L. Guo, P. Han, L. Chuan Guo, Y.Q. Cao, A.D. Li, J.Z. Kong, H.F. Zhai, D. Wu, The antibacterial activity of Ta-doped ZnO nanoparticles. Nanoscale. Res. Lett. **10**, 336 (2015)

43. A. Jain, R. Bhargava, P. Poddar, Probing interaction of Gram-positive and Gram-negative bacteria cells with ZnO nanorods. Mater. Sci. Eng. **33**, 1247–1253 (2013)

44. R. Wahab, A. Mishra, S. IlYun, I.H. Hwang, J. Mussarat, A.A. Al-Khedhairy, Y.S. Kim, H.S. Shi, Fabrication, growth mechanism and antibacterial activity of ZnO micro-spheres prepared via solution process. Biomass Bioenergy **39**, 227–236 (2012)

45. M. Rai, A. Yadav, A. Gade, Silver nanoparticles as a new generation of antimicrobials. Biotechnol. Adv. **27**, 76–83 (2009)

46. A.A. Tayel, W.F. El-tras, S. Moussa, A.F. El-baz, H. Mahrous, M.F. Salem, L. Brimer, Antibacterial action of zinc oxide nanoparticles against food borne pathogens. J. Food Saf. **31**, 211–218 (2011)